Surface science analysis of GaAs photocathodes following sustained electron beam delivery

V. Shutthanandan,[1] Z. Zhu,[1] M. L. Stutzman,[2] F. E. Hannon,[2] C. Hernandez-Garcia,[2] M. I. Nandasiri,[1] S. V. N. T. Kuchibhatla,[1] S. Thevuthasan,[1] and W. P. Hess[3]

[1]*Environmental Molecular Sciences Laboratory, Pacific Northwest National Laboratory, Richland, Washington 99352, USA*
[2]*Thomas Jefferson National Accelerator Facility, Newport News, Virginia 23606, USA*
[3]*Chemical and Materials Science Division, Pacific Northwest National Laboratory, Richland, Washington 99352, USA*

(Received 6 September 2011; published 12 June 2012)

Degradation of the photocathode materials employed in photoinjectors represents a challenge for sustained operation of nuclear physics accelerators and high power free electron lasers (FEL). Photocathode quantum efficiency degradation is due to residual gases in the electron source vacuum system being ionized and accelerated back to the photocathode. These investigations are a first attempt to characterize the nature of the photocathode degradation, and employ multiple surface and bulk analysis techniques to investigate damage mechanisms including sputtering of the Cs-oxidant surface monolayer, other surface chemistry effects, and ion implantation. Surface and bulk analysis studies were conducted on two GaAs photocathodes, which were removed from the JLab FEL DC photoemission gun after delivering electron beam, and two control samples. The analysis techniques include helium ion microscopy, Rutherford backscattering spectrometry (RBS), atomic force microscopy, and secondary ion mass spectrometry (SIMS). In addition, two high-polarization strained superlattice GaAs photocathode samples, one removed from the continuous electron beam accelerator facility (CEBAF) photoinjector and one unused, were also analyzed using transmission electron microscopy (TEM) and SIMS. It was found that heat cleaning the FEL GaAs wafer introduces surface roughness, which seems to be reduced by prolonged use. The bulk GaAs samples retained a fairly well organized crystalline structure after delivering beam but show evidence of Cs depletion on the surface. Within the precision of the SIMS and RBS measurements, the data showed no indication of hydrogen implantation or lattice damage from ion back bombardment in the bulk GaAs wafers. In contrast, SIMS and TEM measurements of the strained superlattice photocathode show clear crystal damage in the wafer from ion back bombardment.

DOI: 10.1103/PhysRevSTAB.15.063501 PACS numbers: 41.60.Cr

I. INTRODUCTION

Scientific productivity at user-based electron accelerators depends on robust photocathode operation to generate high electron beam current, as is the case with high power free electron lasers (FELs), or highly polarized continuous wave (CW) electron beams for nuclear physics research. The photocurrent from a CW laser-irradiated photocathode is given by

$$i = \eta P_{\text{laser}} \frac{e\lambda}{hc},$$

where i is current (A), η is quantum efficiency, P_{laser} is incident laser power (W), λ is laser wavelength (m), e is elementary charge (C), and h is Plank's constant (J s). This shows that the quantum efficiency of a photocathode is dependent not only on the power of the laser, but also on the wavelength (assuming the work function condition is met). When the quantum efficiency (QE) falls below usable levels, beam delivery must be interrupted to replenish or replace the photocathode. The goal of this work is to analyze the surface morphology, composition, and crystalline quality of negative electron affinity GaAs photocathodes used to produce hundreds or thousands of coulombs of charge in DC photoemission guns, in order to better understand the degradation mechanisms. Increasing operational lifetime through understanding photocathode damage mechanisms can help focus future improvements for the electron sources and could improve accelerator availability in both machines at Jefferson Lab (JLab) and elsewhere.

In this work, two types of GaAs-based photocathodes, used in the two accelerators at Jefferson Lab (JLab), have been analyzed; the IR-VUV FEL and the continuous electron beam accelerator facility (CEBAF). The IR-VUV FEL operates with up to 10 mA CW of unpolarized electron beam current obtained from a 350 kV DC photoemission electron gun that uses "bulk" (epi-ready) GaAs photocathodes [1]. CEBAF uses a 100 kV DC photoemission electron gun with strained superlattice GaAs photocathodes to achieve electron beam polarization over 85% at beam currents up to 200 μA CW.

There are some difficulties associated with using GaAs in practice. Primarily this type of photocathode is sensitive to poor vacuum conditions, which result in degradation of the yield or QE. However, if ultrahigh vacuum conditions exist, activated cathodes can survive for thousands of hours when not illuminated with laser light [2]. The QE lifetime is also hundreds of hours under DC high voltage with no illumination. It is when the photocathode is illuminated and an electron beam is emitted, that the QE decays over time, supporting the ion back bombardment damage hypotheses. Photocathode QE degradation, of the type seen in the JLab FEL and CEBAF DC photoemission guns, has long been associated with ionization of residual gases in the vacuum chamber and beam line, and their subsequent acceleration into the photocathode material [3–5].

Understanding the relative contributions of surface damage via sputtering of the Cs-oxidant surface monolayer versus the damage due to ion implantation and ion-induced dislocations in the crystal and heat-induced dopant density fluctuations could provide direction for future efforts to improve photocathode lifetime and yield, particularly for the higher currents required for future projects. Although the cathode electrode in the FEL gun does not provide focusing, there is clear evidence of localized QE degradation, particularly in the geometric center of the photocathode as shown in Fig. 1, which corresponds to the electrostatic center of the anode-cathode geometry. The CEBAF gun electrodes are based on Pierce geometry to provide electron beam focusing, which does not strongly focus ions. However, as the laser beam is moved to many spots around the photocathode active area, the accumulation of damage at the electrostatic center from delivering beam from multiple spots leads to significant and nearly irreversible QE degradation at the photocathode electrostatic center, and reversible damage at the illuminated area and on a band between the two locations [3,5].

A. Photocathode procedures

A direct evolution of the original JLab IR-demo FEL 350 kV DC photoemission gun [6], the IR-VUV FEL upgrade version has been in operation since 2003 [7]. In 1992 when the JLab IR FEL was proposed, GaAs photocathodes were chosen for electron beam requirements reasons and because of the in-house experience at CEBAF with polarized photoinjectors. Each photocathode installed in the photoemission gun is a 3.2 cm diameter, bulk GaAs wafer with crystal orientation (100) $\pm$ 5°, 600 μm thick, and Zn doped at $\sim 1 \times 10^{18}$ cm^{-3}. The wafers arrive in hermetically sealed packages.

For installation, a GaAs sample is attached to the end of a 4-ft. long stalk in a clean room by means of indium foil (which melts on heating providing good thermal contact, and acts as glue on cooling) and a tantalum ring that prevents the wafer falling from the stalk during heating. The stalk is then mounted in a hydrogen cleaning chamber [8]. The wafer was heated to 550°C for one hour then hydrogen cleaned at 300°C for 15 minutes and allowed to cool. The stalk with the clean GaAs wafer is then inserted into the photoemission gun for nominal operation. The complete gun assembly is then baked for one week at 250°C to achieve vacuum conditions below 5×10^{-11} Torr. The photocathode wafer is subsequently heat cleaned at 550°C inside the gun for three hours, then cooled to room temperature. Finally, the wafer is activated *in situ*, into a negative electron affinity (NEA) photocathode by a combination of Cs-atom deposition in a low-pressure background of NF_3 (1×10^{-10} Torr) until the photocurrent saturates. In the FEL gun, typical QE values resulting from this activation process are between 5% and 7% at 532 nm for bulk GaAs, although higher QE has been reported elsewhere [9].

The photocathode is nominally illuminated with a frequency-doubled (527 nm), mode-locked Nd:YLF drive laser to generate 135 pC per bunch. Each laser pulse is

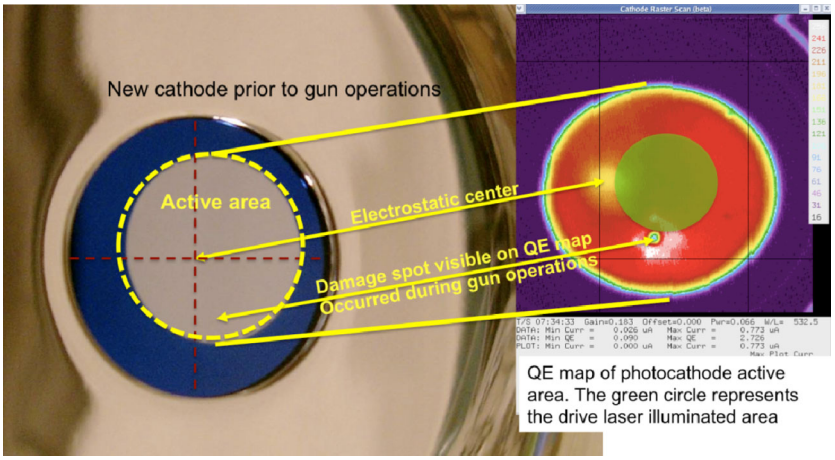

FIG. 1. Photograph and quantum yield map (right) of FEL photocathode. The active area is 16 mm in diameter. The blue region is the anodized area. The laser-illuminated area is the 8 mm diameter shown as the green circle on the quantum yield map.

50 ps FWHM with a transverse top-hat profile 8 mm in diameter. At a repetition rate of 75 MHz, the DC photoemission gun can deliver up to 10 mA CW [10] (limited by the high voltage power supply). The QE decays when electron beam current is extracted from the photocathode during accelerator operation. To compensate for this the drive laser power is increased. When the drive laser can deliver no more power, the photocathode is rejuvenated with a fresh layer of Cs, recovering about 96% of the previous QE. Approximately every 6 recesiations, excessive field emission, observed by a downstream electron beam screen, necessitates a ''heat clean'' and reactivation of the wafer into a NEA photocathode. The reactivation process recovers the original 5%–7% QE and eliminates the field emission, which might be due to accumulation of Cs on the wafer surface. Excessive field emission is problematic for high current FEL operations, as it results in electron beam halo that impacts the beam pipe chamber walls generating undesired radiation and deteriorating vacuum conditions.

With progressive use of the photocathode, the beam halo immediately following the heat clean and reactivation increases. Halo is simply electrons that are emitted from unwanted regions on the photocathode. Eventually, the halo becomes too problematic in downstream regions of the accelerator and the photocathode must be replaced.

The CEBAF photoinjector delivers up to 200 μA of CW polarized electron beam to three experimental halls simultaneously, at the CEBAF accelerator frequency of 1497 MHz. The photocathode (12.8 mm diameter) is illuminated with three frequency-doubled, gain-switched, fiber-coupled seed lasers with ErYb-doped amplifiers, each interleaved at 499 MHz, to provide independent current control for the three experimental halls. The laser beams (~ 0.5 mm diameter FWHM) are moved to new locations across the photocathode when photocathode QE falls to an unacceptable level. The photocathode can support operation from approximately six photocathode locations. After exhausting the QE from the entire photocathode, the sample must be heated and reactivated. The CEBAF photocathode is not recesiated between heat/reactivation cycles.

The CEBAF wafers are delivered from the manufacturer with an arsenic cap, and diced into 1.5 cm squares. The analyzed photocathode was used in a gun similar to, but smaller than, the FEL electron source, with the photocathode mounted on a 26'' long stalk that is inserted into the gun vacuum chamber and baked at 250°C for 30 hours. As with one of the FEL wafers, this CEBAF wafer was anodized in a mild acid solution, which eliminates the QE around a defined active area of the photocathode prior to installation, thus reducing unwanted emission. The strained superlattice photocathodes have only a 100 nm thick photoemitting layer, comprised of 14 periods of 4 nm GaAs interleaved with 3 nm layers of GaAsP to provide strain, which makes ion implantation damage more problematic than in bulk GaAs. The horizontal CEBAF gun was therefore pumped with a large array of nonevaporable getter pumps surrounding the cathode/anode gap to provide maximal pumping in the region resulting in a pressure of 5×10^{-12} Torr in the system that did not significantly change when the valve to the beam line was opened. A heat cycle of $\sim$500°C was found sufficient to activate the photocathode to a QE of over 1% with 780 nm light. Higher temperatures were avoided to minimize dopant migration from the highly doped surface layer.

B. FEL photocathode samples

In 2003, a GaAs wafer (vendor A) delivered over 1000 coulombs in one year of operation and up to 9 mA CW for short periods of time. Because of excessive electron beam halo at 5–8 mA CW, in 2004 it was replaced with a new bulk GaAs wafer grown by a different manufacturer (vendor B). The extracted $1/e$ lifetime was 550 coulombs or 50 operational hours at 5 mA CW. The total extracted charge from that wafer was 7000 coulombs in 900 operational hours with a beam current between 1 and 8.5 mA CW. A fresh layer of Cs was applied to replenish the quantum yield typically once per week. The vendor A wafer underwent 12 heat cleans before removal in 12 months of operation, while the vendor B wafer underwent 9 heat clean cycles in 36 months of operation [10].

C. Polarized photocathode sample

CEBAF uses strained superlattice photocathodes to produce highly polarized electron emission by illumination with circularly polarized light just over the band gap energy. Strain, induced by growing GaAs on a lattice-mismatched substrate [11], breaks the degeneracy between two states in the valance band. If illuminated with a light source that excites electrons exclusively from the upper state, 100% polarized emission is theoretically possible. To increase electron yield and maintain high polarization, photocathodes are now grown in a strained superlattice structure using 14 paired layers of GaAs/GaAsP and a final highly doped GaAs surface layer to reduce surface charge limit effects [12]. Typical polarization from these photocathodes, illuminated with circularly polarized light at 780 nm, has been measured at over 85%. The sample analyzed delivered over 600 coulombs of polarized electrons over a period of approximately 6 months and was heated and reactivated 6 times, with beam delivered to the halls for over 2600 hours during that time.

D. Sample identification and surface analyses

For the work presented here, a total of six GaAs wafer samples were analyzed. The two superlattice wafers analyzed were from the same manufacturing run, with one having delivered 600 coulombs and the other unused. Two

TABLE I. List of photocathode history.

Sample	Manufacturer	Coulombs delivered	Heat cycles	Operating current	Charge lifetime (coulombs)	CW beam time (hrs)	Time in gun (months)	AFM roughness (nm)	Preparation
1000 C	A	1000	12	Up to 8 mA	130	130	12	4.6	Isopropanol, acetone, DI, H cleaned
7000 C	B	7000	9	1–8 mA	550	900	36	4.0	Anodized, isopropanol, acetone, DI, H cleaned
Heated bulk	A	0	1	0	Not applicable	0	0	5.5	
Unused bulk	B	0	0	0	Not applicable	0	0	0.2	
Used superlattice	SVT [11]	600 polarized	6	100–200 μA	~100	~2500	6		Anodized
Unused superlattice	SVT [11]	0	1	0	Not applicable	0	0		As cap removal

bulk wafers, from different manufacturers, used in the JLab FEL DC electron gun were analyzed years after being removed from the system along with two bulk GaAs control samples. The vendor A wafer was installed in the FEL gun in 2003 without further treatments and delivered a total of 1000 coulombs. Prior to installation in 2004, a new wafer from vendor B was first anodized with a mixture of deionized water and 85% phosphoric acid to form a thick oxide layer, effectively eliminating the QE outside the intended use area. In Fig. 1, the wafer anodized area shows in dark blue. The wafer from vendor B delivered a total of 7000 coulombs.

The following list describes each sample, (summarized in Table I): (i) unused bulk GaAs sample from vendor B; (ii) heated bulk GaAs sample not used in the DC gun, from vendor A; (iii) NEA activated bulk GaAs wafer from vendor A used in the FEL gun from 2003 to 2004, identified as the 1000 coulomb sample; (iv) NEA activated bulk GaAs wafer from vendor B used in the FEL gun from 2004 to 2007, identified as the 7000 coulomb sample; (v) NEA activated GaAs superlattice photocathode in use in the CEBAF gun for 6 months from SVT Associates, Inc. [11]; (vi) unused strained superlattice material from the same batch as sample 5.

II. RESULTS AND DISCUSSION

The FEL samples were analyzed using helium ion microscopy (HIM), Rutherford backscattering spectrometry (RBS), atomic force microscopy (AFM), and time of flight secondary ion mass spectrometry (TOF-SIMS). In both the control and the heated samples, most analyses were performed at the geometrical center of the samples. For used photocathode samples, analyses were made at a location within the drive laser-illuminated region (see Fig. 1). The superlattice GaAs samples were analyzed using transmission electron microscopy (TEM) and SIMS, with the cross sectional depth samples prepared by an FIB (focused ion beam) milling and lift-out technique. SIMS analysis was measured at various locations across both samples.

A. Helium ion microscopy and atomic force microscopy

Helium ion microscopy was used to image photocathode surface morphology. HIM is very similar to scanning electron microscopy (SEM) except that it uses He^+ as a probe instead of electrons [13], and has several advantages over SEM. For example, the depth of field is higher in HIM than SEM and the interaction volume is much smaller such that very high resolution images can be obtained (current instrument resolution is 0.35 nm). Furthermore, an electron beam can be used as a charge neutralizer for insulating samples, thus carbon coating of the sample, as is often done in SEM, is not necessary. HIM images were obtained using 25 keV helium ions with 5 pA beam current at normal incidence. Secondary electrons and backscattered ions were detected using Everhart-Thornley and microchannel plate detectors, respectively.

HIM images of the four bulk GaAs FEL photocathode samples are shown in Fig. 2. It is clear from these images that the surface underwent roughening, due to heating [compare Figs. 2(a) and 2(b)]. The heated but unused wafer [Fig. 2(b)] shows interconnected surface nanostructures with an average size of 50 nm. It is known that high temperature heating of GaAs in vacuum induces excess evaporation of As and growth of Ga clusters on the surface [14,15]. Usually these processes are studied at temperatures above 550°C and the material is thought to remain stoichiometric when heated below the noncongruent evaporation temperature of 625°C [14]. Figure 2 clearly shows a systematic variation in the topography of the samples as a function of heat treatment and prolonged photoinjector use, which seems to develop smaller surface nanostructures. AFM images from these samples provide quantitative roughness data and are quite similar to the HIM results. Table I shows the average roughness obtained from AFM measurements for each sample.

The results shown in Table I suggest that the surface roughness does not increase with additional heating cycles and may be reduced by photoinjector operation. The 1000 coulomb sample suffered more damaging events than the 7000 coulomb sample and therefore needed

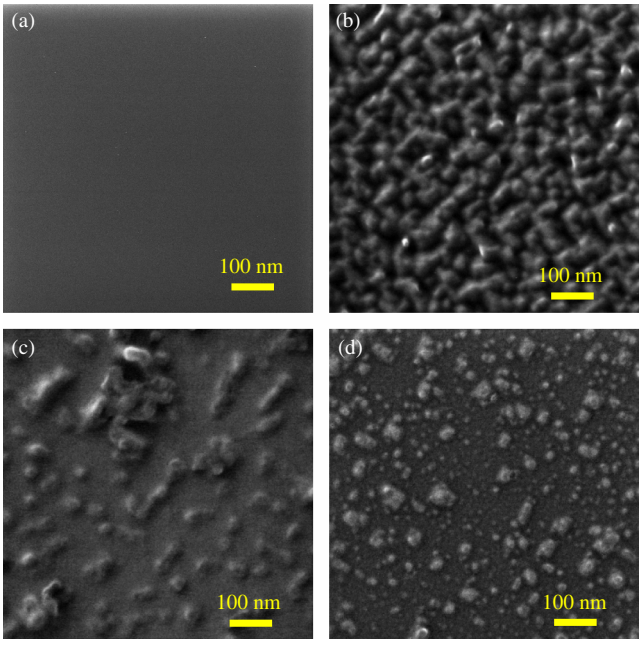

FIG. 2. Comparison of HIM images collected at normal incidence from the four FEL photocathode samples: (a) control, (b) control that has been heated as in the photocathode activation procedure, (c) 1000 coulomb sample, and (d) 7000 coulomb sample.

more heat clean cycles. Since the damage described in the ''FEL photocathode samples'' section is localized for each arcing event, it seems to be unrelated to the surface roughness outside those specific sites.

B. Rutherford backscattering spectrometry

Rutherford backscattering spectrometry (RBS) has been extensively used to investigate stoichiometry, structure, and thickness of thin films and bulk materials [16–18]. In RBS, the probe is typically a He^+ ion beam of energy between ~0.5 and ~2.0 MeV. In this energy regime, coulomb scattering of the incident ion and nuclei in the solid can be treated classically and reasonably accurate numerical simulations can be performed. RBS is element specific as the energy of the backscattered He^+ ion is dependent on the mass of the scatterer at a particular scattering angle. Since the ion loses energy as it travels through the target material, an energy spectrum of the backscattered ions also yields chemical information about the depth at which a given backscattering event occurs. Since high-energy ion beams penetrate deeply into materials, RBS can be used to study buried interfaces and diffusion profiles. RBS spectra were obtained using 2 MeV He^+ ions under channeling and random geometries. The backscattered spectra were collected using a silicon surface barrier detector at a scattering angle of 150°. The incident beam diameter was 1 mm. A detailed description of the RBS experimental setup is reported elsewhere [19].

RBS in channeling geometry probes both surface and bulk material order, such as crystallinity, and is also useful in characterizing defects or damage structures, and impurity or dopant lattice site locations in single crystal materials. In channeling geometry, the incident ion beam is aligned with the low index direction of the crystal surface and can penetrate between atomic rows such that the energy spectrum of backscattered ions exhibits a surface peak (SP) associated with backscatter from atoms in the topmost layers [Fig. 3]. Because of shadowing by the surface layer, the ions that do not scatter from the surface penetrate deep within the crystal without scattering, such that the backscattering yield from the bulk of the crystal is very low.

When the atoms in the surface region are displaced from their original lattice position, due to surface structural change, the SP intensity is expected to increase compared to the value corresponding to the clean, undamaged (well-ordered) surface. In addition, if there is disorder in the near surface region or in the bulk, due to ion implantation or some other means, the channeling will be disrupted and the incident ion beam will be scattered by the displaced (interstitial) or implanted atoms. As a result, the backscattering yield from the atoms in a disordered or damaged region will give rise to a damage feature in the channeling spectrum [see Fig. 3] [16,20]. In random geometry, RBS provides a direct means for measuring the thickness and stoichiometry of a single crystal thin film when the ion beam is incident on the sample at angles other the low index direction of the crystal (usually obtained with the beam incident 7° off normal while the sample is rotated).

RBS measurements were performed along channeling and random geometries within the drive laser-illuminated

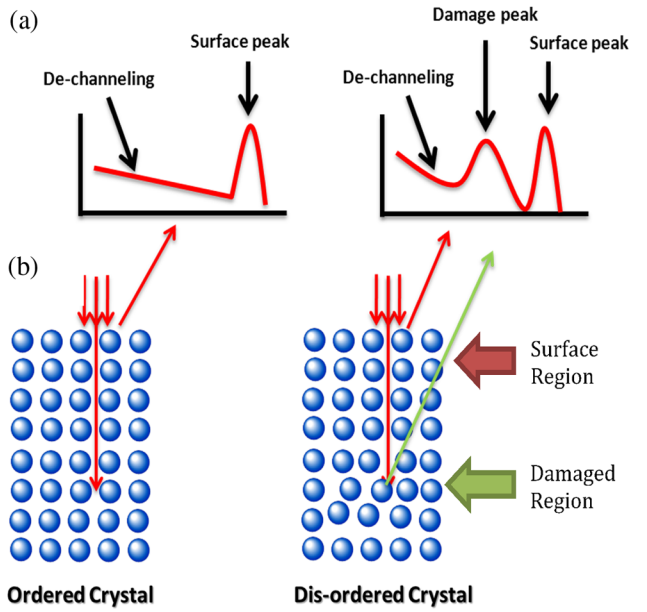

FIG. 3. Schematic of RBS spectra of channeling scattering mechanisms in ordered and disordered single crystals.

region on control, 1000 and 7000 coulomb samples. The channeling spectra are shown in the Fig. 4. The peaks observed at channel number 850 are due to surface cesium. Surface peaks corresponding to both Ga and As are clearly visible in the channeling spectra. The Cs signal is significantly greater on the 1000 coulomb sample than the 7000 coulomb sample. The results shown in Fig. 4 indicate that the 1000 coulomb sample is disordered more in the laser-illuminated region compared to the 7000 coulomb sample. This result is consistent with other results obtained from AFM (smaller average roughness for the 7000 coulomb sample compared to the 1000 coulomb sample) and HIM (smaller nanostructures for the 7000 coulomb sample compared to the 1000 coulomb sample) measurements. It is interesting to note that overall dechanneling in the control sample is slightly higher compared to both the 1000 and the 7000 coulomb samples. One would expect less dechanneling in this sample since the surface shows virtually no clusters and a very small average roughness. It is possible that the control sample may have some residual strain incorporated during crystal growth or polishing. On the 1000 and 7000 coulomb samples, this strain could have been reduced by heat treatment during the photocathode activation procedure.

The minimum yield ratio ($\chi_{\min}$) is the ratio between the backscattered ion yields in the channeling and random geometries. The ($\chi_{\min}$) ratio is usually measured near the minimum following the surface peak and is useful in characterizing crystalline quality. A low $\chi_{\min}$ value, on the order of 3%, indicates the sample is well ordered. The results shown in Fig. 5 further indicate that the quality of the crystal in the laser-illuminated region is

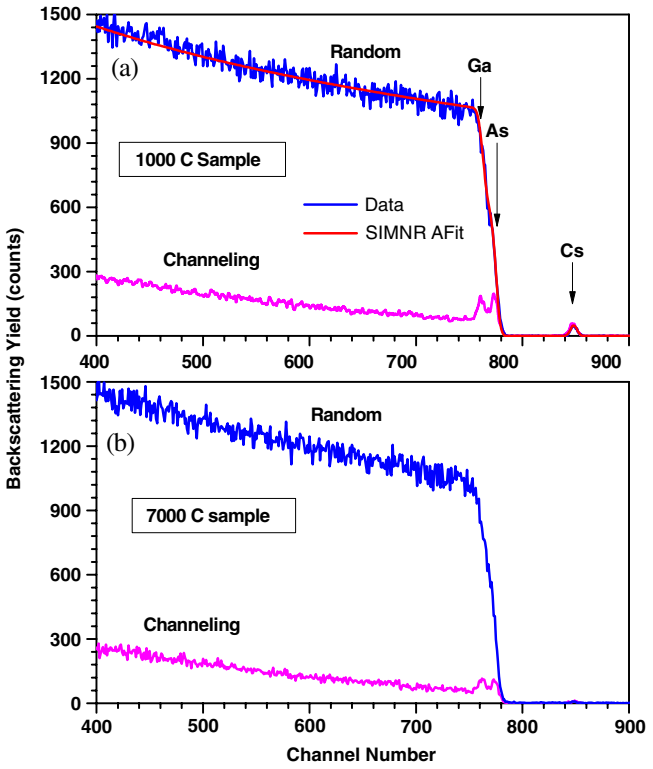

FIG. 5. Comparison of channeling and random RBS spectra (magenta and blue lines, respectively) for the 1000 coulomb sample obtained within the drive laser-illuminated region near the electrostatic center. The red line compares the RBS experimental random spectrum with the SIMNRA simulation. (b) Comparison of channeling and random RBS spectra (magenta and blue lines, respectively) for the 7000 coulomb sample obtained within the drive laser-illuminated region near the electrostatic center.

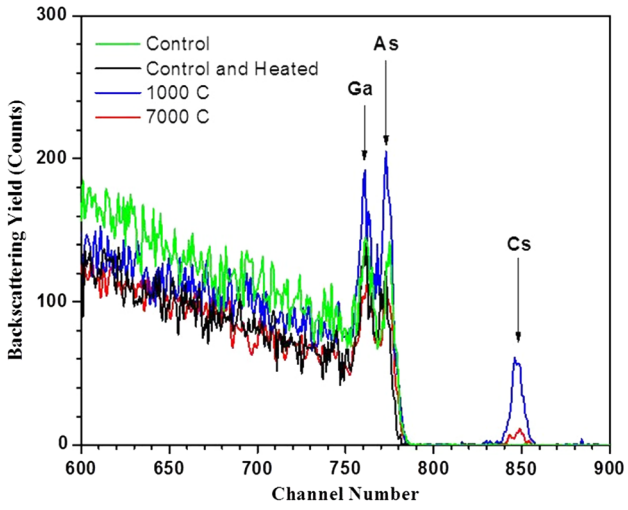

FIG. 4. Channeling Rutherford backscattering spectra of control, heated control, 1000, and 7000 coulomb samples (green, black, blue, and red lines, respectively) taken within the drive laser-illuminated region near the electrostatic center shows the expected surface composition, with peaks due to Ga, As, and Cs.

not affected strongly by morphology changes under prolonged use. The minimum yields ($\chi_{\min}$) obtained for 1000 coulomb and the 7000 coulomb samples are 7.4% and 4.8%, respectively (for the heated and unheated control samples these values are 4.5 and 5.0%, respectively). These values indicate considerable crystal order, with respect to the bulk of the crystal, even though these surfaces display well-defined nanostructures. RBS can also quantify submonolayer levels of ultrathin films for large Z elements such as Cs. RBS was used to quantify surface Cs in the 1000 coulomb and the 7000 coulomb samples [Figs. 5(a) and 5(b)]. The SIMNRA simulation program [21] was used to model the experimental RBS spectra collected along the random geometry to determine the stoichiometry of the GaAs single crystals as well as the surface Cs coverage. The arrows in Fig. 5(a) indicate the energetic positions expected for backscattering from Cs, As, and Ga surface atoms. Based on SIMNRA simulations, the Cs surface concentrations were determined to be 1.75×10^{15} at/cm^2 for the 1000 coulomb sample and 0.4×10^{15} at/cm^2 for 7000 coulomb

sample. These results are consistent with the history of each sample. The 1000 coulomb sample was NEA reactivated two days before being removed from the electron gun and still had a substantial QE ($\sim 2\%$) left, while the 7000 coulomb sample was NEA reactivated about 2 weeks before being removed from the electron gun and its QE was below 0.1% prior to removal. The correlation between Cs concentration and QE of each sample prior to removal from the gun supports a QE degradation mechanism based on Cs loss due to ion back-bombardment sputtering.

It is believed that hydrogen ion back bombardment causes the photocathode QE to degrade with use. If the loss of QE is due to bulk wafer damage induced by ion back bombardment, then we would expect to observe damage peaks in the channeling spectrum (Fig. 3). Calculations indicate that hydrogen implantation should peak at a depth of 1.5 μm which, in turn, should lead to a damage feature near channel 450. The channeling spectra (Fig. 5) do not show any evidence of damage peaks. It is possible that bulk damage caused by hydrogen back bombardment is repaired somewhat during the heat cleaning and reactivation process, although implanted hydrogen would be expected to be retained inside the sample. We attempted SIMS depth profiling to detect implanted hydrogen. The SIMS depth profiles show no evidence of hydrogen implantation and we conclude that hydrogen concentrations in all the samples are lower than our detection limit of 1×10^{18} atoms/cm^3.

C. Secondary ion mass spectrometry

Time of flight (TOF) secondary ion mass spectrometry (SIMS) was used to study photocathode surface contamination. Although SIMS is not regarded as a quantitative technique, it is known to have ppm to ppb sensitivity for trace elements. TOF-SIMS measurements were performed using a TOF-SIMS 5 spectrometer (IONTOF GmbH, Münster, Germany) equipped with a 25 keV bismuth (Bi) cluster ion source, a 10 keV $C_{60}{}^+$ source, and a 0.2–2.0 keV $Cs^+/O_2{}^+$ sputtering source. For depth profiling, the sample was sputtered using a 2.0 keV Cs^+ beam for negative ion analysis, or a 2.0 keV $O_2{}^+$ beam for positive ion analysis.

Positive ion SIMS spectra from all FEL samples were obtained at several characteristic mass to charge ratios. TOF-SIMS shows that the major components in all these samples are Ga and As with trace impurities of Na, Mg, Al, Si, K, and Ca in the laser-illuminated region. The alkali metals, Na and K, are found to be evenly distributed on smooth surfaces, while Mg, Al, Si, Ca, and In ions show higher concentrations on particles and microscopic scratches. TOF-SIMS is very sensitive to Na, K, Ca, and Al, but not to Mo, Pb, and Zn. In addition, Zn is close enough in mass to Ga to make Zn detection even less sensitive. An analysis report provided by the Cs strip vendor (SAES Getters) accounts for the presence of Na, K, Ca, Al, Mo, Pb, and Zn as present in the Cs dispenser that is used for photocathode activation. In addition, it is clear that the 1000 coulomb sample displays a much larger Cs surface concentration than does the 7000 coulomb sample. Figure 6 shows TOF-SIMS images of Cs smoothly distributed on both the 1000 and 7000 coulomb samples. The measured Cs surface concentrations are consistent with those determined by RBS.

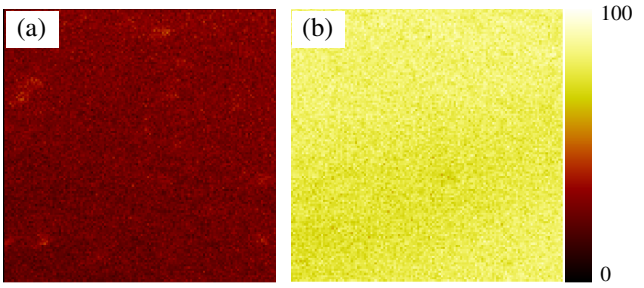

FIG. 6. Positive ion SIMS images obtained from (a) 7000 coulomb and (b) 1000 coulomb samples showing relative Cs concentrations. The total number of Cs ion counts are, respectively, 4.33×10^5 and 1.295×10^6, consistent with RBS data that determined the Cs surface concentrations to be 1.75×10^{15} at/cm^2 for the 1000 coulomb sample and 0.4×10^{15} at/cm^2 for the 7000 coulomb sample. The field of view in both (a) and (b) is 150 μm $\times$ 150 μm.

D. Strained superlattice analysis

Transmission electron microscopy (TEM) was used to study the damage of the strained superlattice photocathode sample. Sample preparation for TEM analysis of the strained superlattice structure was performed at North Carolina State University using a focused ion beam (FIB) milling and a lift-out technique to prepare the samples without damaging the superlattice structure [22]. To remove the depth cross section for TEM analysis, the GaAs is first protected by coating with an evaporative layer of gold and palladium. This is followed by a layer of platinum sputter coated with the FIB, followed by FIB milling of the sample. The TEM images obtained from the strained superlattice photocathodes (used and unused control samples) are shown in Fig. 7. TEM images clearly show the layers of the superlattice in cross section. While lattice dislocations are evident in both images, areas of significant darkening, typical of ion implantation damage, including possible strain relaxation, can be seen in the CEBAF sample [Fig. 7(a)] but not in the unused control sample [Fig. 7(b)]. The damage region is nonuniform across the surface of the material at this length scale. The laser spot is $\sim$500 μm diameter, far larger than the distance scales observed on this TEM image. The nature of this nonuniformity is not understood at this time.

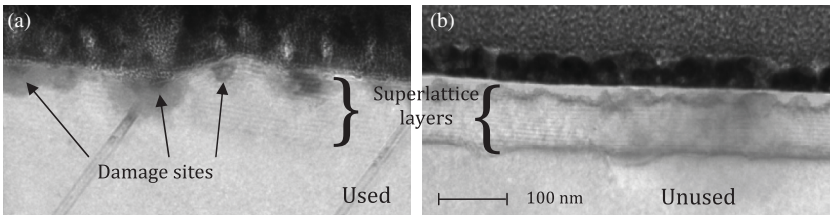

FIG. 7. TEM images of used (left) and unused (right) superlattice photocathode material. The dark areas at the top are the Au/Pd and Pt protective layers. The 100 nm thick superlattice of 3 and 4 nm layers of GaAs/GaAsP can be seen. The used cathode shows deep ''stains'', which are not evident in the unused sample on the right. Blurring at the top of the unused cathode is due to a slight tilt during TEM imaging which images the gold overlayer as well as the cathode.

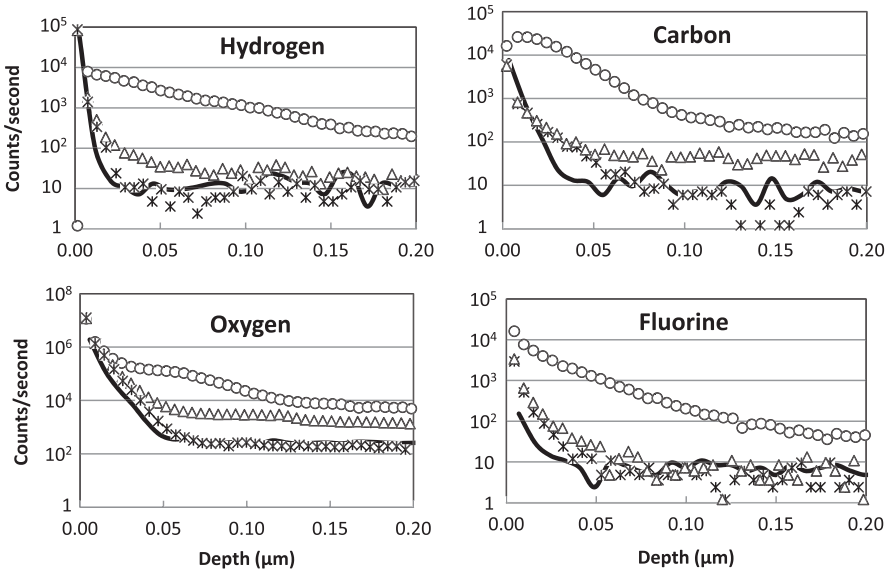

FIG. 8. SIMS analysis of the unused (solid line) and used strained superlattice wafers (open data points) show an increase in implantation as a function of depth for most SIMS analysis positions on the photocathode. Positions were unable to be directly correlated to operational positions, but for all species, open circles (o) are believed to be at the electrostatic center, data indicated by an *x* is believed to be from a minimally damaged region and data indicated in triangles from an intermediate region. Note that the strained superlattice structure is only 100 nm thick, and implantation is seen both in and deeper than the strained superlattice structure.

Figure 8 displays SIMS depth profiles for oxygen, hydrogen, carbon, and fluorine for the unused and used CEBAF superlattice photocathode samples. The SIMS analysis for the superlattice photocathodes used a 1.875 kV Cs^+ ion beam, 160 micron raster size, sputtering rate of 0.5 nm/second, with parameters chosen to be as sensitive to hydrogen implantation as possible. The black line indicates the SIMS signal strength for each element from one representative milling site in the unused sample. SIMS data was measured at seven locations across the used sample, and most data followed one of two trends: either slight implantation near the surface and little implantation beyond (data indicated by crosses) or moderate implantation at all depths (data indicated by triangles). Representative data sets for these two conditions are shown. One location yielded high readings in all species (shown in circles), and is believed to be near the electrostatic center where ions are more likely to implant when running at any beam position.

Hydrogen is the primary residual gas in the UHV vacuum system and is expected to implant, but the damage due to hydrogen ion implantation may be limited due to its low mass. Carbon and oxygen are present in the system due largely to the chemistry in ion pumps which can show residual gas spectra with CH_4, CO, and CO_2. Note the oxygen count rates are 3 orders of magnitude higher than the other signals, partially due to the much higher sensitivity of the method for oxygen. The fluorine trace is present due to residual NF_3 in the system from the activation of the photocathode. Since the size of the SIMS ion beam is much larger than the scale of the damage sites on the TEM image, determining the elemental composition of the various implantation sites or the degree of implantation per layer is very difficult.

III. CONCLUSIONS

In an effort to better understand quantum efficiency degradation mechanisms in bulk and superlattice GaAs photocathodes, several samples that delivered many coulombs in DC photoemission guns have been analyzed using HIM, AFM, RBS, TOF-SIMS, TEM, and SIMS. These results suggest that ion back bombardment, commonly recognized as the main degradation mechanism, can cause sputtering of the Cs monolayer and/or crystal damage.

What is interesting about our findings is that the FEL photocathodes in the 350 keV gun showed evidence of Cs sputtering, but not of ion-induced crystal damage, at least within the resolution of the measurements. The correlation found by the RBS measurements between Cs concentration and QE of each sample prior to removal from the gun supports the Cs sputtering by ion back bombardment as a QE degradation mechanism. The combination of SIMS and RBS measurements should have indicated crystal dislocations or hydrogen implantation due to back bombardment if present, but the data showed no evidence of this. Conversely, the TEM analysis of the CEBAF strained superlattice photocathodes showed areas of significant darkening, typical of ion implantation damage in the used photocathode. SIMS measurements of the used CEBAF photocathode found implanted hydrogen, oxygen, and carbon and fluorine atoms, at varied levels across the photocathode surface, due to backscattering in the 100 kV DC CEBAF gun. Cs sputtering was not investigated as a damage mechanism for the CEBAF samples.

Because of the small number of samples, our results are not unequivocal, but rather serve as motivation to further studies. For example, it is thought that thermal effects are responsible for repairing some of the damage induced by back-accelerated ions implanted into the photocathode material during operation. Measurements at JLab using bulk GaAs indicate that extended heating (12 hours rather than 2 hours at 525°C) is significantly more effective in rejuvenating the QE and maximum yield in both bulk and strained superlattice photocathodes, particularly in heavily damaged areas such as the electrostatic center [23].

Of more profound consequences to high brightness photocathodes are the results confirming previous observations of surface nanostructure formation induced by heating during the cleaning step in the activation of negative electron affinity photocathodes. The Cornell group has studied the effect of surface morphology on thermal emittance, of similarly treated GaAs photocathodes, showing that their analytical model for photoemission predicts their emittance measurements when the surface roughness is included in the model [24]. Unfortunately, at the moment there are no means to characterize the effect of the surface morphology changes on the electron beam emittance at the JLab FEL.

It is interesting to note that the FEL photocathodes remained crystalline after prolonged use. In addition, surface roughness appears to be most strongly correlated to the initial heat treatment, although we cannot quantify changes to roughness due to additional heating and cleaning cycles. The coulombs of beam delivered or time in the gun may be factors in the reduced roughness observed in used samples. These factors indicate that the heating and cleaning cycle should be evaluated to prolong the use of a photocathode in the FEL. Since the number of available samples for analyses was limited, a further study on a separate cathode preparation chamber would be valuable in answering these questions.

Proposed next generation light sources [25] will be capable of generating spatially and temporally coherent x-ray beams with unprecedented photon brightness, on the order of 10^{21}–10^{25} photons/s/mm^2/mr^2 0.1% bandwidth, at photon energies between 10^1–10^3 eV [26]. The predicted photon brightness is ultimately limited by the electron beam normalized transverse emittance at the undulator, which in turn is limited by the thermal emittance of the photocathode [27]. Developing a process to preserve the native surface quality of the GaAs wafer could be a significant contribution to low emittance photocathodes [24,27]. For example, GaAs wafers can be manufactured with an arsenic cap that prevents surface contamination. This cap layer is easily removed by gentle heating at temperatures well below 500°C. Gentle arsenic decapping under UHV conditions should therefore produce a flat and clean surface ideal for the first NEA photocathode activation. Although this would render a one-time-use photocathode, having an electron gun with a load-lock chamber storing several photocathodes would minimize the machine down time during cathode changeout and would provide high brightness beam.

Alternate cleaning methods such as hydrogen cleaning performed at lower temperatures can be used effectively in cleaning the surface of bulk GaAs photocathodes [28,29]. Oxide contaminants can be removed by high temperature heating of the GaAs sample, but carbides cannot be removed via heat. Hydrogen cleaning effectively removes carbon and oxygen contamination from the GaAs surface, and is performed typically around 300°C, which is not hot enough to cause surface roughening. Unfortunately, this method is not effective for the more easily damaged strained superlattice GaAs photocathode [30]. One more alternative could be to develop a program for studying the effectiveness of UV laser light in removing oxides and carbides without altering the photocathode surface morphology and chemical composition.

In the case of the superlattice photocathode used in CEBAF, TEM results show a clear indication of ion implantation, and the SIMS analysis shows the presence of the expected residual gases in the deep-UHV vacuum system. Scanning TEM combined with energy dispersive x-ray analysis could shed light on the composition of the implantation sites to determine the distribution of the

species detected in the SIMS analysis. If one is able to determine the species implanting and affecting the QE degradation, this information would allow tailoring the emphasis of improvements for the DC high voltage electron gun vacuum system.

ACKNOWLEDGMENTS

A significant portion of this work was performed using the Environmental Molecular Sciences Laboratory (EMSL), a national scientific user facility sponsored by the Department of Energy's Office of Biological and Environmental Research and located at Pacific Northwest National Laboratory (PNNL). PNNL is operated by Battelle for the U.S. Department of Energy under Contract No. DE-AC05-76RL01830. The EMSL part of the work was funded by a PNNL LDRD program. Financial support for the FEL photocathode electron gun work was provided by the Office of Naval Research, the Army Night Vision Laboratory, the Air Force Research Laboratory, the Joint Technology Office, the Commonwealth of Virginia, and by the U.S. DOE Basic Energy Sciences under Contract No. DE-AC05-060R23177. M. L. Stutzman would like to acknowledge the help of collaborators at North Carolina State University, Dr. Fred Stevie and Dr. Dale Batchelor, for the surface analysis techniques used with the strained superlattice photocathode and interpretation of the results. The authors also wish to acknowledge the help of Dr. Matt Poelker for his useful suggestions to the production of this paper. This manuscript has been authored by Jefferson Science Associates, LLC under Contract No. DE-AC05-06OR23177 with the U.S. Department of Energy.

[1] D. Engwall, C. Bohn, L. Cardman, B. Dunham, D. Khene, R. Legg, H. Liu, M. Shinn, and C. Sinclair, in *Proceedings of the 1997 Particle Accelerator Conference, Vancouver, BC* (IEEE, Piscataway, NJ, 1998), p. 2693.

[2] C. K. Sinclair, P. A. Adderley, B. M. Dunham, J. C. Hansknecht, P. Hartmann, M. Poelker, J. S. Price, P. M. Rutt, W. J. Schneider, and M. Steigerwald, Phys. Rev. ST Accel. Beams **10**, 023501 (2007).

[3] K. Aulenbacher, Proceedings of the Workshop on Photocathodes for Polarized Electron Sources for Accelerators (SLAC-R-432, 1993).

[4] E. Pozdeyev, Phys. Rev. ST Accel. Beams **10**, 083501 (2007).

[5] J. Grames, R. Suleiman, P. A. Adderley, J. Clark, J. Hansknecht, D. Machie, M. Poelker, and M. L. Stutzman, Phys. Rev. ST Accel. Beams **14**, 043501 (2011).

[6] T. Siggins, C. Sinclair, C. Bohn, D. Bullard, D. Douglas, A. Grippo, J. Gubeli, G. A. Krafft, and B. Yunn, Nucl. Instrum. Methods Phys. Res., Sect. A **475**, 549 (2001).

[7] C. Hernandez-Garcia, T. Siggins, S. Benson, D. Bullard, H. F. Dylla, K. Jordan, C. Murria, G. R. Neil, M. Shinn, and R. Walker, in *Proceedings of the 21st Particle Accelerator Conference, Knoxville, 2005* (IEEE, Piscataway, NJ, 2005), pp 3117–3119 [http://accelconf.web.cern.ch/accelconf/p05/PAPERS/WPAP050.PDF].

[8] E. Petit, F. Houzay, and J. M. Moison, J. Vac. Sci. Technol. A **10**, 2172 (1992).

[9] N. Nishimori, I. Bazarov, B. Dunham, J. Grames, C. Hernandez-Garcia, L. Jones, B. Militsyn, M. Poelker, K. Surles-Law, and M. Yamamoto, in Proceedings of Energy Recovery Linac Conference 2009, ERL09, Ithaca, New York, USA, 2009, p. 6 [http://accelconf.web.cern.ch/accelconf/ERL2009/papers/wg102.pdf].

[10] C. Hernandez-Garcia, S. V. Benson, G. Biallas, J. Boyce, D. Bullard, J. Coleman, D. Douglas, P. Evtushenko, C. Gould, A. Grippo, J. Gubeli, F. Hannon, D. Hardy, M. Kelley, J. Kortze, K. Jordan, J. M. Klopf, M. Marchlik, W. Moore, G. R. Neil, T. Powers, D. Sexton, M. Shinn, C. Tennant, R. Walker, G. Williams, and S. Zhang, in Proceedings of Energy Recovery Linac Conference 2009, ERL09, Ithaca, New York, USA, 2009, p. 37 [http://accelconf.web.cern.ch/accelconf/ERL2009/papers/wg107.pdf].

[11] T. Maruyama *et al.*, Appl. Phys. Lett. **85**, 2640 (2004) [http://www.svta.com]; J. E. Clendenin, in *Proceedings to the 10th Workshop on Polarized Sources and Targets, Novosibirsk, Russia, 2003* [Nucl. Instrum. Methods Phys. Res., Sect. A, 536, 308 (2005)].

[12] T. Maruyama, A. Brachmann, J. E. Clendenin, T. Desikan, Edward L. Garwin, R. E. Kirby, D. A. Luh, C. Y. Prescott, J. Turner, and R. Prepost, AIP Conf. Proc. **675**, 1083 (2003).

[13] L. Scipioni, C. A. Sanford, J. Notte, B. Thompson, and S. McVey, J. Vac. Sci. Technol. B **27**, 3250 (2009).

[14] J. Tersoff, D. E. Jesson, and W. X. Tang, Science **324**, 236 (2009).

[15] T. D. Lowes and M. Zinke-Allmang, J. Appl. Phys. **73**, 4937 (1993).

[16] L. C. Feldman and J. W. Mayer, *Fundamentals of Surface and Thin Film Analysis* (North-Holland, New York, 1986).

[17] S. A. Chambers, C. M. Wang, S. Thevuthasan, T. Droubay, D. E. McCready, A. S. Lea, V. Shutthanandan, and C. F. Windisch, Thin Solid Films **418**, 197 (2002).

[18] V. Shutthanandan, S. Thevuthasan, Y. Liang, and E. M. Adams, Appl. Phys. Lett. **80**, 1803 (2002).

[19] S. Thevuthasan, C. H. F. Peden, M. H. Engelhard, D. R. Baer, G. S. Herman, W. Jiang, Y. Liang, and W. J. Weber, Nucl. Instrum. Methods Phys. Res., Sect. A **420**, 81 (1999).

[20] V. Shutthanandan, A. A. Saleh, and R. J. Smith, Surf. Sci. **450**, 204 (2000).

[21] M. Mayer, *Max-Planck-Institut für Plasmaphysik, Garching, Germany, 2008*, SIMNRA User's Guide 6.04.; M. Mayer, in *Proceedings of the 15th International Conference on the Application of Accelerators in Research and Industry, Denton, TX, 1998*, edited by J. L. Duggan and I. L. Morgan, AIP Conf. Proc. No. 475 (American Institute of Physics, New York, 1999), p. 541.

[22] F. A. Stevie, C. B. Vartuli, L. A. Giannuzzi, T. L. Shofner, S. R. Brown, B. Rossie, F. Hillion, R. H. Mills, M. Antonell, R. B. Irwin, and B. M. Purcell, Surf. Interface Anal. **31**, 345 (2001).

[23] J. Grames (private communication).
[24] S. Karkare and I. Bazarov, Appl. Phys. Lett., **98**, 094104 (2011).
[25] BES Advisory Committee Report [http://www.er.doe.gov/bes/reports/files/NGPS_rpt.pdf], 2009.
[26] Reports No. ANL-08/39, No. BNL-81895-2008, No. LBNL-1090E-2009, and No. SLAC-R-197.
[27] D. H. Dowell, I. Bazarov, B. Dunham, K. Harkay, C. Hernandez-Garcia, R. Legg, H. Padmore, T. Rao, J. Smedley, and W. Wan, Nucl. Instrum. Methods Phys. Res., Sect. A **622**, 685 (2010).
[28] C. K. Sinclair, B. M. Poelker, and J. S. Price, in Proceedings of the 1997 Particle Accelerator Conference, Vancouver, BC (Ref. [1]), p. 2864.
[29] T. Maruyama, D.-A. Luh, A. Brachmann, J. E. Clendenin, E. L. Garwin, S. Harvey, R. E. Kirby, and C. Y. Prescott, R. Prepost, Appl. Phys. Lett. **82**, 4184 (2003).
[30] M. Baylac, P. Adderley, J. Brittian, J. Clark, T. Day, J. Grames, J. Hansknecht, M. Poelker, M. Stutzman, and A. T. Wu, Phys. Rev. ST Accel. Beams **8**, 123501 (2005).